

Prediction of the analyzing power for $\vec{p}+{}^6\text{He}$ elastic scattering at 200 MeV from $\vec{p}+{}^4\text{He}$ elastic scattering at 200 MeV

Masahiro Ishii,^{1,*} Yasunori Iseri,^{2,†} and Masanobu Yahiro^{1,‡}

¹*Department of Physics, Graduate School of Sciences, Kyushu University, Fukuoka 819-0395, Japan*

²*Chiba-Keizai College, Chiba 263-0021, Japan*

(Dated: January 4, 2022)

We apply the cluster-folding (CF) model for $\vec{p}+{}^6\text{He}$ scattering at 200 MeV, where the potential between \vec{p} and ${}^4\text{He}$ is fitted to data on $\vec{p}+{}^4\text{He}$ scattering at 200 MeV. For $\vec{p}+{}^6\text{He}$ scattering at 200 MeV, the CF model reproduces measured differential cross section with no free parameter. We then predict the analyzing power $A_y(q)$ with the CF model, where q is the transfer momentum. Johnson, Al-Khalili and Tostevin construct a theory for one-neutron halo scattering, taking (1) the adiabatic approximation and (2) neglecting the interaction between a valence neutron and a target, and yield a simple relationship between the elastic scattering of a halo nucleus and of its core under certain conditions. We improve their theory with (3) the eikonal approximation in order to determine $A_y(q)$ for ${}^6\text{He}$ from the data on $A_y(q)$ for ${}^4\text{He}$. The improved theory is accurate, when approximation (1)–(3) are good. Among the three approximations, approximation (2) is most essential. The CF model shows that approximation (2) is good in $0.9 \lesssim q \lesssim 2.4 \text{ fm}^{-1}$. In the improved theory, the $A_y(q)$ for ${}^6\text{He}$ is the same as that for ${}^4\text{He}$. In $0.9 \lesssim q \lesssim 2.4 \text{ fm}^{-1}$, we then predict $A_y(q)$ for $\vec{p}+{}^6\text{He}$ scattering at 200 MeV from measured $A_y(q)$ for $\vec{p}+{}^4\text{He}$ scattering at 200 MeV. We thus predict $A_y(q)$ with the model-dependent and the model-independent prescription. The ratio of differential cross sections measured for ${}^6\text{He}$ to that for ${}^4\text{He}$ is related to the wave function of ${}^6\text{He}$. We then determine the radius between ${}^4\text{He}$ and the center-of-mass of valence two neutrons in ${}^6\text{He}$. The radius is 5.77 fm.

PACS numbers: 24.10.Ht, 24.70.+s, 25.40.Cm, 25.60.Bx, 29.25.Pj

I. INTRODUCTION

In the framework of the shell model for nuclei, the central and spin-orbit potentials are important for understanding nuclear structure. The importance was first discovered by Mayer and Jensen. The central and spin-orbit potentials in various stable nuclei are similar to the real part of optical potential in the \vec{p} elastic scattering on the corresponding stable nuclei. The optical potentials are well determined by measured differential cross sections $d\sigma/d\Omega$ and analyzing powers A_y .

In general, the central and spin-orbit potentials in the scattering of unstable nuclei on a \vec{p} target are different from the case of stable nuclei, since unstable nuclei have larger radii than the stable nuclei with the common mass number [1, 2].

For scattering of ${}^6\text{He}$ on a \vec{p} target at an incident energy $E_{\text{lab}} = 71 \text{ MeV}$, the A_y was obtained in the inverse measurement [3–5]. In the experiment, the $d\sigma/d\Omega$ is measured in $1.1 \lesssim q \lesssim 2.2 \text{ fm}^{-1}$ ($42^\circ \lesssim \theta_{\text{cm}} \lesssim 87^\circ$) and the A_y is in $1.0 \lesssim q \lesssim 1.9 \text{ fm}^{-1}$ ($37^\circ \lesssim \theta_{\text{cm}} \lesssim 74^\circ$) [3–5], where q and θ_{cm} are the transfer momentum and the scattering angle in the center-of-mass frame, respectively. The measured A_y is reproduced by the cluster-folding (CF) model [5]. It is shown in Ref. [5] that the spin-orbit part of the phenomenological optical potential has a shallow and long-ranged shape. This problem is not solved yet.

The same measurement was made for $E_{\text{lab}} = 200 \text{ MeV}$ [6], since the nucleon-nucleon (NN) total cross section has a min-

imum around there. However, the result was shown only for $d\sigma/d\Omega$ in $1.7 \lesssim q \lesssim 2.7 \text{ fm}^{-1}$ ($36^\circ \lesssim \theta_{\text{cm}} \lesssim 59^\circ$).

The $\vec{p}+{}^4,6\text{He}$ scattering at $E_{\text{lab}} = 200 \text{ MeV}$ were analyzed by the Melbourne g-matrix folding model [1]. The model predicted $d\sigma/d\Omega$ and A_y for ${}^6\text{He}$, but not does account for the data [7] for ${}^4\text{He}$ in $q \gtrsim 3.3 \text{ fm}^{-1}$ ($\theta_{\text{cm}} \gtrsim 80^\circ$). *Ab initio* folding potentials based on no-core shell-model [8] were constructed and applied for $\vec{p}+{}^4,6\text{He}$ scattering at $E_{\text{lab}} = 200 \text{ MeV}$. The model reproduces the data on $d\sigma/d\Omega$ for ${}^6\text{He}$, but not $d\sigma/d\Omega$ for ${}^4\text{He}$ in $q \gtrsim 2.5 \text{ fm}^{-1}$ ($\theta_{\text{cm}} \gtrsim 60^\circ$).

Crespo and Moro calculated $d\sigma/d\Omega$ and A_y for the $\vec{p}+{}^4,6,8\text{He}$ scattering at $E_{\text{lab}} = 297 \text{ MeV}$, using the Multiple Scattering expansion [9]. Microscopic optical potentials derived from NN t matrix and nonlocal density was applied to the $\vec{p}+{}^4\text{He}$ scattering at $E_{\text{lab}} = 200 \text{ MeV}$ [10], and reproduced the data of Ref. [7] in $q \lesssim 4.1 \text{ fm}^{-1}$ ($\theta_{\text{cm}} \lesssim 110^\circ$).

Johnson, Al-Khalili and Tostevin constructed a theory, using the adiabatic approximation and neglecting the interaction between a valence neutron and a target for one-neutron halo scattering [11]. They yield a simple relationship between the elastic scattering of a halo nucleus and of its core from a stable target. The relation is good, if (1) the adiabatic approximation is accurate and (2) the potential between a valence neutron and a target can be switched off. In the present paper, we refer to the theory of Ref. [11] as valence-core cutting (VCC) theory. When the VCC theory is applied to $\vec{p}+{}^6\text{He}$ scattering, the relation is Eq. (11) in Sec. II.

In this paper, we improve the VCC theory for $\vec{p}+{}^6\text{He}$ scattering at $E_{\text{lab}} = 71$ and 200 MeV, using (3) the eikonal approximation in addition to approximations (1) and (2). Among the approximations, approximation (2) is most essential and should be investigated. Using the CF mode, we confirm that approximation (2) is good in $0.9 \lesssim q \lesssim 2.4 \text{ fm}^{-1}$ for $E_{\text{lab}} =$

*ishii@phys.kyushu-u.ac.jp

†iseri@chiba-kc.ac.jp

‡yahiro@phys.kyushu-u.ac.jp

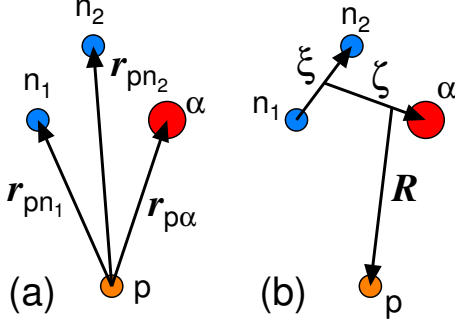


FIG. 1: Two sets of coordinates in four-body model.

200 MeV, but good only in the vicinity of $q = 0.9 \text{ fm}^{-1}$ for $E_{\text{lab}} = 71 \text{ MeV}$.

In the improved VCC theory, the A_y for ${}^6\text{He}$ is the same as that for ${}^4\text{He}$. In $0.9 \leq q \leq 2.4 \text{ fm}^{-1}$, we can predict $A_y(q)$ for $\vec{p}+{}^6\text{He}$ scattering at 200 MeV from $A_y(q)$ measured for $\vec{p}+{}^4\text{He}$ scattering at 200 MeV without using any model. Since the ratio of $d\sigma/d\Omega$ for ${}^6\text{He}$ to that for ${}^4\text{He}$ is related to the wave function of ${}^6\text{He}$, we can determine the radius between ${}^6\text{He}$ and the center-of-mass of valence two neutrons from the ratio.

In order test to approximation (2), we use the CF model for $\vec{p}+{}^6\text{He}$ scattering at 200 MeV, where the potential between \vec{p} and ${}^4\text{He}$ is fitted to data on $\vec{p}+{}^4\text{He}$ scattering at 200 MeV. The CF model reproduces the differential cross section for $\vec{p}+{}^6\text{He}$ scattering with no free parameter. We then predict A_y .

The improved VCC theory and the results are shown in Sec. II. The CF model is explained and its results are shown in Sec. III. Section IV is devoted to a summary.

II. IMPROVED VCC THEORY AND ITS RESULTS

We start with the $p+n_1+n_2+{}^4\text{He}$ four-body model to consider the \vec{p} elastic scattering on ${}^6\text{He}$ at $E_{\text{lab}} = 71$ and 200 MeV; see Fig. 1 for two coordinate sets of the four-body system. The total Hamiltonian of the scattering is

$$H = -\frac{\hbar^2}{2\mu_6} \nabla_R^2 + U + H_6, \quad (1)$$

$$U = U_{pn_1}(r_{pn_1}) + U_{pn_2}(r_{pn_2}) + U_{p\alpha}(r_{p\alpha}) + V_{p\alpha}^{\text{Coul}}(r_{p\alpha}) \quad (2)$$

where μ_6 is the reduce mass between \vec{p} and ${}^6\text{He}$ and the Hamiltonian H_6 of ${}^6\text{He}$ is described by the $n_1+n_2+{}^4\text{He}$ three-body model. The coordinates $r_{p\gamma}$ for $\gamma = n_1, n_2, \alpha$ are shown in Fig. 1 (a). The $U_{p\gamma}$ are the nuclear interaction between \vec{p} and γ .

The exact T -matrix of the elastic scattering is

$$T = \langle e^{i\mathbf{k}\cdot\mathbf{R}}\Phi | U | \Psi \rangle \quad (3)$$

for the total wave function Ψ , the incident momentum \mathbf{k} . The ground state Φ of ${}^6\text{He}$ has an energy ε_0 .

Following Ref. [11], we take the adiabatic approximation to the total wave function Ψ and neglect the interactions U_{pn_1} and U_{pn_2} . The resulting Hamiltonian is

$$H_{\text{AD}} = -\frac{\hbar^2}{2\mu_6} \nabla_R^2 + U_{p\alpha}(r_{p\alpha}) + V_{p\alpha}^{\text{Coul}}(r_{p\alpha}) + \varepsilon_0, \quad (4)$$

$$= -\frac{\hbar^2}{2\mu_6} \nabla_{r_{p\alpha}}^2 + U_{p\alpha}(r_{p\alpha}) + V_{p\alpha}^{\text{Coul}}(r_{p\alpha}) + \varepsilon_0, \quad (5)$$

where $\nabla_R^2 = \nabla_{r_{p\alpha}}^2$ as a result of the transform from \mathbf{R} to $r_{p\alpha}$. The initial wave function of Ψ is

$$e^{i\mathbf{k}\cdot\mathbf{R}}\Phi = e^{i\mathbf{k}\cdot(\mathbf{r}_{p\alpha} - \alpha_{vc}\zeta)}\Phi \quad (6)$$

with $\alpha_{vc} = 2/(4+2) = 1/3$. We then obtain

$$T_{\text{AD}} = \langle e^{i\mathbf{k}\cdot\mathbf{R}}\Phi | U_{p\alpha} + V_{p\alpha}^{\text{Coul}}(r_{p\alpha}) | e^{-i\alpha_{vc}\mathbf{k}\cdot\zeta}\Phi\chi_{\mathbf{k}}(r_{p\alpha}) \rangle \quad (7)$$

with the distorting wave function $\chi_{\mathbf{k}}(r_{p\alpha})$ defined by

$$\chi_{\mathbf{k}}(r_{p\alpha}) = \frac{i\varepsilon}{E_{\text{cm}} - \frac{\hbar^2}{2\mu_6} \nabla_{r_{p\alpha}}^2 + U_{p\alpha}(r_{p\alpha}) + V_{p\alpha}^{\text{Coul}}(r_{p\alpha}) + i\varepsilon} e^{i\mathbf{k}\cdot\mathbf{r}_{p\alpha}} \quad (8)$$

with infinitesimally small ε and the incident energy $E_{\text{cm}} = \hbar^2 k^2 / (2\mu_6)$ in the center of mass system. The $\chi_{\mathbf{k}}(r_{p\alpha})$ is the distorting wave function between \vec{p} and ${}^4\text{He}$ with the reduced mass μ_6 , and not the distorting wave function of the $\vec{p}+{}^4\text{He}$ elastic scattering with the same incident energy E_{lab} , because the reduced mass μ_6 between \vec{p} and ${}^6\text{He}$ is different from the reduced mass μ_4 between \vec{p} and ${}^4\text{He}$.

The T_{AD} becomes

$$T_{\text{AD}} = F(\alpha_{vc}(\mathbf{k} - \mathbf{k}')) \langle e^{i\mathbf{k}'\cdot\mathbf{r}_{p\alpha}} | U_{p\alpha} + V_{p\alpha}^{\text{Coul}} | \chi_{\mathbf{k}}(r_{p\alpha}) \rangle_{r_{p\alpha}} \quad (9)$$

with the form factor

$$F(\mathbf{Q}) \equiv F(\alpha_{vc}(\mathbf{k} - \mathbf{k}')) = \langle e^{i\alpha_{vc}(\mathbf{k} - \mathbf{k}')\cdot\zeta} | \Phi \rangle_{\zeta}^2 \quad (10)$$

for $\mathbf{Q} \equiv \alpha_{vc}(\mathbf{k} - \mathbf{k}') = \mathbf{q}/3$.

Using Eq. (9), we can get the differential cross section as

$$\left(\frac{d\sigma}{d\Omega} \right)_{p+{}^6\text{He}} = |F(\mathbf{Q})|^2 \left(\frac{d\sigma}{d\Omega} \right)_{p+{}^4\text{He}}^{\mu_6}. \quad (11)$$

This equation was derived in Ref. [11]. In the right hand side of Eq. (11), the part $\left(\frac{d\sigma}{d\Omega} \right)_{p+{}^4\text{He}}^{\mu_6}$ is calculated theoretically [11].

Now we improve Eq. (11) in order to determine $|F(\mathbf{Q})|$ from experimental data on $\vec{p}+{}^4,{}^6\text{He}$ scattering at the same E_{lab} . The incident energy E_{lab} in the laboratory system is determined by the velocity v as

$$E_{\text{lab}} = \frac{v^2 M_p}{2} \quad (12)$$

for proton mass M_p . When we apply the eikonal approximation to the $p+{}^4\text{He}$ scattering, the scattering amplitude is

$$f_{p\alpha} = \frac{i\mu_4 v}{2\pi\hbar} \int d\mathbf{b} e^{-i\mathbf{q}\cdot\mathbf{b}} (1 - e^{i\chi(\mathbf{b})}) \quad (13)$$

with

$$\chi(\mathbf{b}) = -\frac{1}{\hbar v} \int_{-\infty}^{\infty} dz [U_{p\alpha}(z, \mathbf{b}) + V_{p\alpha}^{\text{Coul}}(z, \mathbf{b})] \quad (14)$$

for $\mathbf{r}_{p\alpha} = (\mathbf{b}, z)$. The differential cross section is thus determined by v , i.e., E_{lab} . We then obtain

$$\left(\frac{d\sigma}{d\Omega}\right)_{p+{}^6\text{He}}^{E_{\text{lab}}} = |F(\mathbf{Q})|^2 \left(\frac{d\sigma}{d\Omega}\right)_{p+{}^4\text{He}}^{E_{\text{lab}}} \left(\frac{\mu_6}{\mu_4}\right)^2. \quad (15)$$

from Eqs. (13)-(14). The equation (15) allows us to determine $|F(\mathbf{Q})|$ from two differential cross sections measured for $\vec{p}+{}^4\text{He}$ and $\vec{p}+{}^6\text{He}$ scattering at a common E_{lab} .

When p is polarized, the factor $(|F(\mathbf{Q})|_{\mu_6/\mu_4})^2$ is common between the cross section for incident proton having up-spin and that for proton having down-spin. This means that the vector analyzing $A_y(q)$ for $\vec{p}+{}^6\text{He}$ scattering is the same as $A_y(q)$ for $\vec{p}+{}^4\text{He}$ in the improved VCC theory.

The relation (15) between $\left(\frac{d\sigma}{d\Omega}\right)_{p+{}^6\text{He}}^{E_{\text{lab}}}$ and $\left(\frac{d\sigma}{d\Omega}\right)_{p+{}^4\text{He}}^{E_{\text{lab}}}$ is good, when the eikonal and adiabatic approximations are good and $U_{pn_1} = U_{pn_2} = 0$. It is shown in Ref. [16] that the eikonal and adiabatic approximations are good for a few hundred MeV. The approximation $U_{pn_1} = U_{pn_2} = 0$ is good in $0.9 \lesssim q \lesssim 2.4 \text{ fm}^{-1}$ for 200 MeV as shown in Sec. III B, but good only near $q = 0.9 \text{ fm}^{-1}$ for 71 MeV as mentioned in Sec. III C.

A. Determination of $|F|$ from measured differential cross sections for $\vec{p}+{}^{4,6}\text{He}$ scattering

Using Eq. (15), we can determine $|F(Q)|$ from experimental data on the cross sections of $p+{}^{4,6}\text{He}$ scattering at the same E_{lab} , when the most essential condition $U_{pn_1} = U_{pn_2} = 0$ is good and the angular momentum between n_1 and n_2 is zero.

As for $E_{\text{lab}} = 200 \text{ MeV}$, the data are available in Ref. [7] for ${}^4\text{He}$ and in Ref. [6] for ${}^6\text{He}$. As for $E_{\text{lab}} = 71 \text{ MeV}$, the data are available in Refs. [5, 17] for ${}^6\text{He}$, but not for ${}^4\text{He}$. We then take the data [18] on $\vec{p}+{}^4\text{He}$ scattering at $E_{\text{lab}} = 72 \text{ MeV}$. The resulting $|F(Q)|$ is smooth, as shown in Fig. 2. The approximation $U_{pn_1} = U_{pn_2} = 0$ is good in $0.9 \lesssim q \lesssim 2.4 \text{ fm}^{-1}$ for 200 MeV as shown in Sec. III B, but good only in the vicinity of $q = 0.9 \text{ fm}^{-1}$ for 71 MeV as mentioned in III C. In Fig. 2, the resulting $|F(Q)|$ is thus reliable in $0.3 \lesssim Q \lesssim 0.8 \text{ fm}^{-1}$.

The Fourier transform $|F(\zeta)|$ of $|F(Q)|$ is a function of ζ . We then assume that the potential between ${}^4\text{He}$ and the center-of-mass of n_1 and n_2 is a one-range Gauss function $V(\zeta)$, and can obtain $|F(Q)|$ by solving Schrodinger equation with the potential. The solid line denotes a result of $V(\zeta) = -25 \exp[-(\zeta/1.41)^2]$, and reproduces the experimental $|F(Q)|$ for 200 MeV. The resulting radius between ${}^4\text{He}$ and the center-of-mass of n_1 and n_2 is 5.77 fm. The corresponding binding energy is 0.172 MeV.

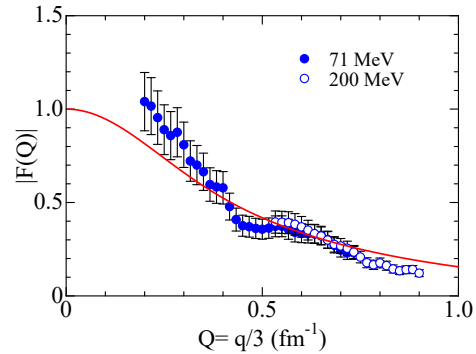


FIG. 2: Q dependence of $|F|$. The solid (open) circles are the result determined from the experimental data at 71 (200) MeV. The solid line is a result of $V(\zeta) = -25 \exp[-(\zeta/1.41)^2]$. Experimental data are taken from Refs. [5, 17, 18] for 71 MeV and Refs. [6, 7] for 200 MeV.

B. Model independent prediction on A_y for $\vec{p}+{}^{4,6}\text{He}$ scattering at 200 MeV

When p is polarized, the factor $|F(\alpha_{vc}(\mathbf{k} - \mathbf{k}'))|_{\mu_6/\mu_4}$ is common between the cross section for incident proton having up-spin and that for proton having down-spin. This means that the vector analyzing $A_y(q)$ for $\vec{p}+{}^6\text{He}$ scattering is the same as $A_y(q)$ for $\vec{p}+{}^4\text{He}$, when the condition $U_{pn_1} = U_{pn_2} = 0$ is good. As mentioned later in Sec. III B, the condition is well satisfied in $0.9 \lesssim q \lesssim 2.4 \text{ fm}^{-1}$.

We make a model-independent prediction on $A_y(q)$ for ${}^6\text{He}$, assuming that the $A_y(q)$ for ${}^6\text{He}$ is the same as the measured $A_y(q)$ of Ref. [7] for ${}^4\text{He}$. The predicted $A_y(q)$ can be transformed into $A_y(\theta)$.

Figure 3 shows the predicted $A_y(\theta)$ for ${}^6\text{He}$. The predicted $A_y(\theta)$ is reliable in $20^\circ \lesssim \theta_{\text{cm}} \lesssim 55^\circ$ ($0.9 \lesssim q \lesssim 2.4 \text{ fm}^{-1}$). The reliable prediction in $20^\circ \lesssim \theta_{\text{cm}} \lesssim 55^\circ$ are denoted by closed circles. It should be noted that our prediction shown by open circles are not good.

C. A_y for 71 MeV

Figure 4 shows q dependence of A_y measured for $\vec{p}+{}^4\text{He}$ scattering at $E_{\text{lab}} = 72 \text{ MeV}$ and that for $\vec{p}+{}^6\text{He}$ scattering at $E_{\text{lab}} = 71 \text{ MeV}$. The A_y for ${}^6\text{He}$ is close to that for ${}^4\text{He}$, except for a data at $q = 1.71 \text{ fm}^{-1}$. The property can be analyzed quantitatively by the Jensen-Shannon (JS) divergence [21]. We show the analysis in Appendix A, since the analysis is new but has recently been used by LIGO Scientific and Virgo Collaborations [22].

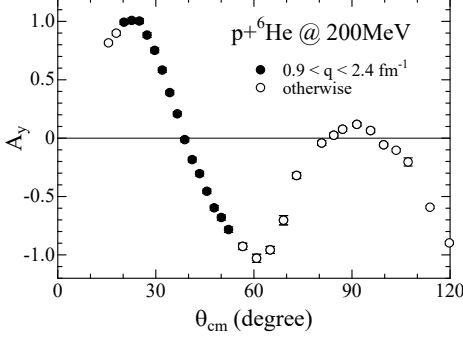


FIG. 3: θ dependence of predicted A_y for $\vec{p}+{}^6\text{He}$ scattering at 200 MeV. See the text for closed and open circles.

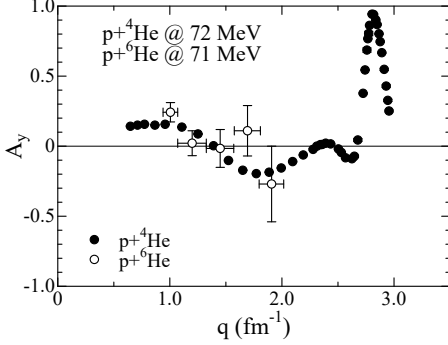


FIG. 4: q dependence of measured A_y (closed circles) for $\vec{p}+{}^4\text{He}$ scattering at $E_{\text{lab}} = 72$ MeV and measured A_y (open circles) for $\vec{p}+{}^6\text{He}$ scattering at $E_{\text{lab}} = 71$ MeV. Data are taken from Ref. [5] for ${}^6\text{He}$ and Ref. [18] for ${}^4\text{He}$.

III. CLUSTER-FOLDING MODEL

We consider the cluster folding (CF) model for the \vec{p} elastic scattering from ${}^6\text{He}$ at $E_{\text{lab}} = 200$ MeV. In addition, we recalculate the \vec{p} elastic scattering from ${}^6\text{He}$ at $E_{\text{lab}} = 71$ MeV in order to obtain the F .

Following Ref. [5], we derive the nuclear potential $U_{\text{CF}}(R)$ between \vec{p} and ${}^6\text{He}$ with the ${}^6\text{He}$ density [19, 20] obtained by αnn OCM:

$$U_{\text{CF}}(R) = \int U_{pn_1} \rho_n^{\text{CF}}(r_1) d\mathbf{r}_1 + \int U_{pn_2} \rho_n^{\text{CF}}(r_2) d\mathbf{r}_2 + \int U_{p\alpha} \rho_\alpha^{\text{CF}}(r_\alpha) d\mathbf{r}_\alpha, \quad (16)$$

with

$$U_{pn_1} = U_{pn_1}^0(r_{pn_1}) + U_{pn_1}^{\text{LS}}(r_{pn_1}) \ell_{pn_1} \cdot (\boldsymbol{\sigma}_p + \boldsymbol{\sigma}_{n_1}), \quad (17)$$

$$U_{pn_2} = U_{pn_2}^0(r_{pn_2}) + U_{pn_2}^{\text{LS}}(r_{pn_2}) \ell_{pn_2} \cdot (\boldsymbol{\sigma}_p + \boldsymbol{\sigma}_{n_2}), \quad (18)$$

$$U_{p\alpha} = U_{p\alpha}^0(r_{p\alpha}) + U_{p\alpha}^{\text{LS}}(r_{p\alpha}) \ell_{p\alpha} \cdot \boldsymbol{\sigma}_p, \quad (19)$$

where the coordinates \mathbf{r}_1 , \mathbf{r}_2 and \mathbf{r}_α are the position vectors of n_1 , n_2 , and the alpha core from the center of mass of ${}^6\text{He}$, respectively, and ρ_n^{CF} and ρ_α^{CF} are the neutron and α densities, respectively.

We can rewrite the $U_{\text{CF}}(R)$ into

$$U_{\text{CF}} = U_0^{\text{CF}}(R) + U_{\text{LS}}^{\text{CF}}(R) \mathbf{L} \cdot \boldsymbol{\sigma}_p, \quad (20)$$

with the central part

$$U_0^{\text{CF}}(R) = 2 \int U_{pn}^0(|\mathbf{r}_1 - \mathbf{R}|) \rho_n^{\text{CF}}(r_1) d\mathbf{r}_1 + \int U_{p\alpha}^0(|\mathbf{r}_\alpha - \mathbf{R}|) \rho_\alpha^{\text{CF}}(r_\alpha) d\mathbf{r}_\alpha \quad (21)$$

and the spin-orbit part

$$U_{\text{LS}}^{\text{CF}}(R) = \frac{1}{3} \int U_{pn}^{\text{LS}}(|\mathbf{r}_1 - \mathbf{R}|) \left\{ 1 - \frac{\mathbf{r}_1 \cdot \mathbf{R}}{R^2} \right\} \rho_n^{\text{CF}}(r_1) d\mathbf{r}_1 + \frac{2}{3} \int U_{p\alpha}^{\text{LS}}(|\mathbf{r}_\alpha - \mathbf{R}|) \left\{ 1 - \frac{\mathbf{r}_\alpha \cdot \mathbf{R}}{R^2} \right\} \rho_\alpha^{\text{CF}}(r_\alpha) d\mathbf{r}_\alpha. \quad (22)$$

In the derivation of Eq. (22), the following points have been used; (I) the internal momenta of ${}^4\text{He}$ and their expectation values are effectively zero for a spherically symmetric nucleus, and (II) the internal coordinates contribute to \mathbf{L} by its component along the \mathbf{R} direction. Eventually we have used

$$\ell_{p\gamma} = C_\gamma \mathbf{L} \left(1 - \frac{\mathbf{r}_\gamma \cdot \mathbf{R}}{R^2} \right) \quad (23)$$

with $C_\gamma = 1/6$ for $\gamma = n_1, n_2$ and $C_\gamma = 2/3$ for $\gamma = \alpha$.

The $U_{p\alpha}$ is the optical potential (OP), and U_{pn_1} and U_{pn_2} are the CEG [12–14]. The g matrix, derived from the Hamada-Johnston potential [15], is successful in reproducing the data on \vec{p} elastic scattering from many nuclei in a wide range of incident energies, $E_{\text{lab}} = 20$ –200 MeV [12–14]. For $\vec{p} + {}^6\text{He}$ elastic scattering at 71 MeV, the CF model well reproduces the data on differential cross sections and A_y [5].

A. Potential fitting of $\vec{p}+{}^4\text{He}$ scattering and results of CF model $\vec{p}+{}^6\text{He}$ scattering

We now fit the OP potential $U_{p\alpha}$ to data [7] for $\vec{p}+{}^4\text{He}$ scattering at $E_{\text{lab}} = 200$ MeV with a Woods-Saxon form:

$$U_{p\alpha} = -V_0 f_r(r_{p\alpha}) - iW_0 f_i(r_{p\alpha}) + 4i a_{id} W_{id} \frac{d}{dr_{p\alpha}} f_{id}(r_{p\alpha}) + V_s \frac{2}{r_{p\alpha}} \frac{d}{dR} f_s(r_{p\alpha}) \ell_{p\alpha} \cdot \boldsymbol{\sigma}_p \quad (24)$$

with

$$f_x(r_{p\alpha}) = \left[1 + \exp\left(\frac{r_{p\alpha} - r_x A^{1/3}}{a_x} \right) \right]^{-1} \quad (25)$$

for $x = r, i, id, s$, where σ_p stands for the Pauli spin operator of an incident proton. The Coulomb potential between the proton and ${}^4\text{He}$ (${}^6\text{He}$) is obtained from the uniformly charged sphere with the radius $1.4A^{1/3}$, where $A = 4$ for ${}^4\text{He}$ and $A = 6$ for ${}^6\text{He}$.

The best-fit potential parameters are obtained by minimizing the χ^2 values of $d\sigma/d\Omega$ and A_y . The resulting parameter set is tabulated in Table I, together with the case of $E_{\text{lab}} = 72$ MeV of Ref. [5].

First of all, we briefly shows results of the OP and the CF model in Fig. 5. The left panel shows that our fitting is good for $\vec{p}+{}^4\text{He}$ scattering at $E_{\text{lab}} = 200$ MeV. The right panel indicates that the CF model reproduces $\vec{p}+{}^6\text{He}$ scattering at $E_{\text{lab}} = 200$ MeV and that the condition $U_{pn_1} = U_{pn_2} = 0$ is good for $d\sigma/d\Omega$ and A_y in $\theta_{\text{cm}} \lesssim 52^\circ$. Now we predict A_y for $\vec{p}+{}^6\text{He}$ scattering at $E_{\text{lab}} = 200$ MeV, using the CF model.

Further analyses based on the improved VCC theory are made below by using q instead of θ_{cm} .

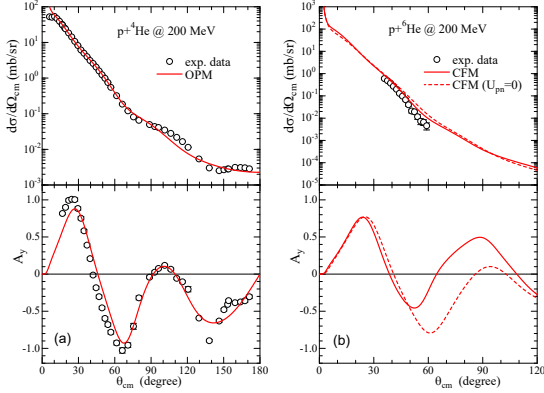


FIG. 5: θ_{cm} dependence of $d\sigma/d\Omega$ and A_y for $\vec{p}+{}^4,6\text{He}$ scattering at $E_{\text{lab}} = 200$ MeV. In left panel, the solid line is a result of our fitting based on the optical potential model (OPM). In the right panel, the solid and dashed lines denote results of CF model (CFM) with and without U_{pn_1} and U_{pn_2} , respectively. Experimental data are taken from Ref. [7] for ${}^4\text{He}$ and Ref [6] for ${}^6\text{He}$.

B. Model-dependent prediction on A_y for $\vec{p}+{}^4,6\text{He}$ scattering at $E_{\text{lab}} = 200$ MeV

Figure 6 shows q dependence of $d\sigma/d\Omega$ for $\vec{p}+{}^4,6\text{He}$ scattering at $E_{\text{lab}} = 200$ MeV in the upper panel and the form factor $|F(Q)|$ in the lower panel. In the upper panel, the CF model (solid line) reproduces the data [6] for $\vec{p}+{}^6\text{He}$ scattering at $E_{\text{lab}} = 200$ MeV with no free parameter. In the lower panel, the solid line denotes the $|F(Q)|$ calculated with the CF-folding model, while U_{pn_1} and U_{pn_2} are switched off in the dashed line. The difference between the two lines shows that effects of U_{pn_1} and U_{pn_2} are small in the region $0.3 \lesssim Q \lesssim 0.8 \text{ fm}^{-1}$ ($0.9 \lesssim q \lesssim 2.4 \text{ fm}^{-1}$).

Figure 7 shows q dependence of A_y for $\vec{p}+{}^6\text{He}$ scattering. The solid line denotes the A_y calculated with the CF-folding

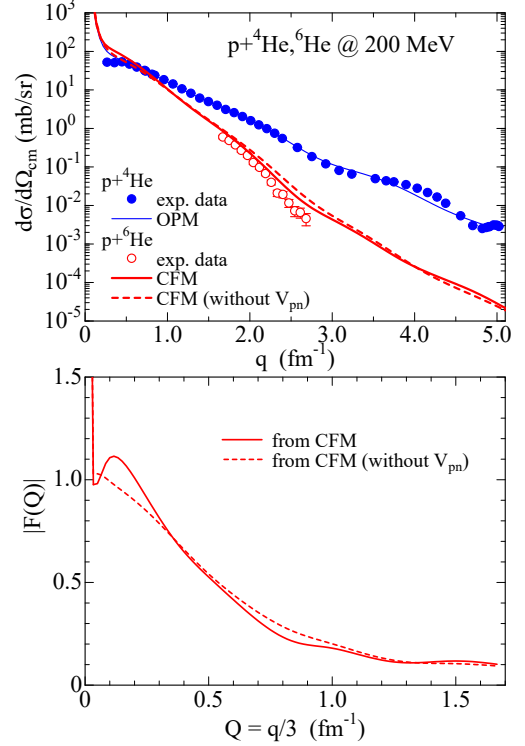


FIG. 6: q dependence of $d\sigma/d\Omega$ for $\vec{p}+{}^4,6\text{He}$ scattering at $E_{\text{lab}} = 200$ MeV in the upper panel and the form factor $|F(Q)|$ in the lower panel. Experimental data are taken from Ref. [7] for $\vec{p}+{}^4\text{He}$ scattering and Ref. [6] for $\vec{p}+{}^6\text{He}$ scattering.

model, while U_{pn_1} and U_{pn_2} are switched off in the dashed line. The difference between the solid and dashed lines show that the condition $U_{pn_1} = U_{pn_2} = 0$ is good in $q \lesssim 2.4 \text{ fm}^{-1}$. Eventually, the condition is good in $0.9 \lesssim q \lesssim 2.4 \text{ fm}^{-1}$, when we see both $d\sigma/d\Omega$ and A_y .

Now we predict A_y for $\vec{p}+{}^6\text{He}$ scattering at $E_{\text{lab}} = 200$ MeV, using the CF model. In $0.9 \lesssim q \lesssim 2.4 \text{ fm}^{-1}$, open circles are the A_y for ${}^6\text{He}$ derived from the measured A_y of Ref. [7] for ${}^4\text{He}$. The CF model reproduces the derived A_y in $0.9 \lesssim q \lesssim 2.0 \text{ fm}^{-1}$.

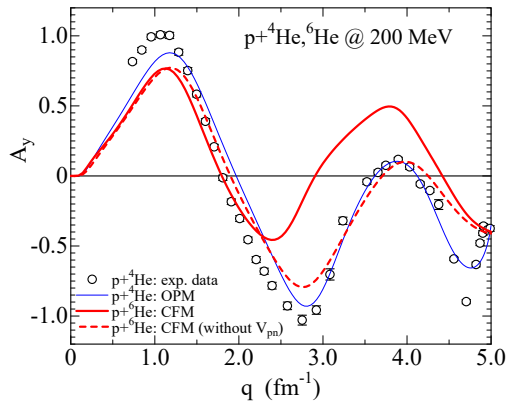
C. CF results on $d\sigma/d\Omega$ and A_y for 71 MeV

Figure 8 shows the results of the CF-model for $d\sigma/d\Omega$ and A_y of $\vec{p}+{}^6\text{He}$ scattering at $E_{\text{lab}} = 71$ MeV in the upper and middle panels. The CF model reproduces the data [4, 5] with no free parameter. The upper and middle panels also show the results of the best optical potential for $d\sigma/d\Omega$ and A_y of $\vec{p}+{}^4\text{He}$ scattering at $E_{\text{lab}} = 72$ MeV.

The lower panel shows the $|F(Q)|$ calculated with the CF model. The difference between the solid and dashed lines indicates that the condition $U_{pn_1} = U_{pn_2} = 0$ is good only in

TABLE I: Parameters of the optical potentials for $\vec{p}+{}^4\text{He}$ scattering at $E_{\text{lab}} = 200$ MeV. For 72 MeV, the parameter set is taken from Ref. [5].

		V_0	r_r	a_r	W_0	r_i	a_i	W_{id}	r_{id}	a_{id}	V_s	r_s	a_s
	(MeV)	(MeV)	(fm)	(fm)	(MeV)	(fm)	(fm)	(MeV)	(fm)	(fm)	(MeV)	(fm)	(fm)
$p+{}^4\text{He}$	200	-26.528	0.7839	0.1446	17.098	1.205	0.5268	—	—	—	6.689	0.8215	0.2641
$p+{}^4\text{He}$	72	54.87	0.8566	0.09600	—	—	—	31.97	1.125	0.2811	3.925	0.8563	0.4914

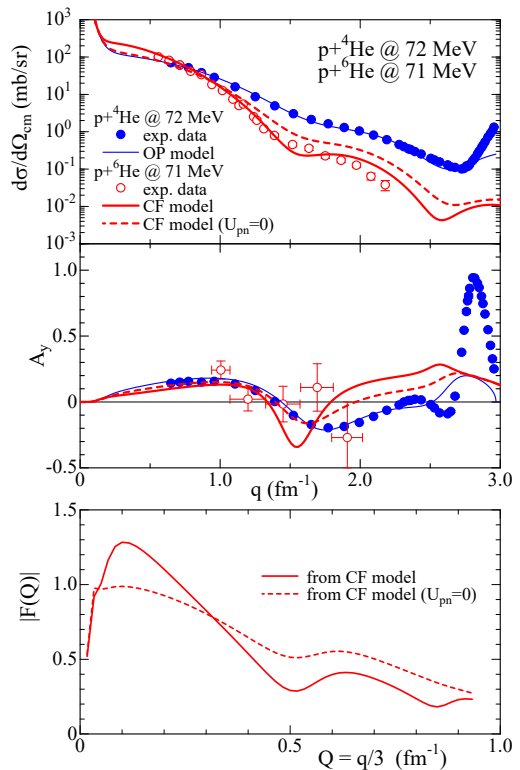

 FIG. 7: q dependence of A_y for $\vec{p}+{}^6\text{He}$ scattering at $E_{\text{lab}} = 200$ MeV. The solid line denotes a result of the CF-folding model, while U_{pn_1} and U_{pn_2} are switched off in the dashed line. The thin solid line is a result of the fitting for $\vec{p}+{}^4\text{He}$ scattering at $E_{\text{lab}} = 200$ MeV. Open circles show the experimental data [7] for $\vec{p}+{}^4\text{He}$ scattering. In $0.9 \leq q \leq 2.4$ fm $^{-1}$, open circles can be regarded as measured A_y for the $\vec{p}+{}^6\text{He}$ scattering at $E_{\text{lab}} = 200$ MeV. Experimental data are taken from Ref. [7] for ${}^4\text{He}$.

the vicinity of $Q = 0.3$ fm $^{-1}$.

IV. SUMMARY

We have applied the cluster-folding (CF) model for $\vec{p}+{}^6\text{He}$ scattering at 200 MeV, where the optical potential between \vec{p} and ${}^4\text{He}$ is fitted to data for $\vec{p}+{}^4\text{He}$ scattering at 200 MeV; see Fig. 5. The CF model reproduces the differential cross section of $\vec{p}+{}^6\text{He}$ scattering with no free parameter. We then predict A_y , as shown in Fig. 7. The solid line is our prediction based on the CF model, while the open circles are our model-independent prediction in $0.9 \leq q \leq 2.4$ fm $^{-1}$.

In order to make the model-independent prediction for $\vec{p}+{}^6\text{He}$ scattering at 200 MeV, we improve the VCC theory, using the eikonal approximation in addition to the $U_{pn_1} = U_{pn_2} = 0$ approximation and the adiabatic approximation. In the improved VCC theory, the A_y for ${}^6\text{He}$ is the same as that for ${}^4\text{He}$. The $U_{pn_1} = U_{pn_2} = 0$ approximation is most essential among the three approximations. Using the CF model, we have confirmed that the $U_{pn_1} = U_{pn_2} = 0$ approximation is good in $0.9 \leq q \leq 2.4$ fm $^{-1}$ for 200 MeV, but good only near


 FIG. 8: q dependence of $d\sigma/d\Omega$ and A_y for $\vec{p}+{}^{4,6}\text{He}$ scattering at $E_{\text{lab}} \approx 71$ MeV in the upper and middle panels and the form factor $|F(Q)|$ in the lower panel. The solid and dashed lines denote results of CF model with and without U_{pn_1} and U_{pn_2} for ${}^6\text{He}$, respectively. The thin solid line denotes the result of fitting for ${}^4\text{He}$. Data are taken from Refs. [5, 17] for ${}^6\text{He}$ and from Ref. [18] for ${}^4\text{He}$.

$q = 0.9$ fm $^{-1}$ for 71 MeV. In $0.9 \leq q \leq 2.4$ fm $^{-1}$, we predict $A_y(q)$ for $\vec{p}+{}^6\text{He}$ scattering at 200 MeV from measured $A_y(q)$ for $\vec{p}+{}^4\text{He}$ scattering at 200 MeV. This is a model-independent prediction in $0.9 \leq q \leq 2.4$ fm $^{-1}$ ($20^\circ \leq \theta_{\text{cm}} \leq 55^\circ$); see Fig. 3.

We thus predict $A_y(q)$ with the model-dependent and the model-independent prescription. Difference between the two predictions is ambiguity of our prediction in $0.9 \leq q \leq 2.4$ fm $^{-1}$.

The ratio $|F(Q)|$ of differential cross sections measured for ${}^6\text{He}$ to that for ${}^4\text{He}$ is related to the wave function of ${}^6\text{He}$. We have then determined the radius between ${}^4\text{He}$ and the center-of-mass of valence two neutrons. The radius is 5.77 fm.

The Jensen-Shannon (JS) divergence [21] is new data analyses used by LIGO Scientific and Virgo Collaborations [22]. The present work is a first application of JS divergence in nuclear physics. Since the analysis is two new, we show it in Appendix A.

Acknowledgments

We would like to thank Prof. Hiyama for providing the numerical data of the ${}^6\text{He}$ density, Dr. Toyokawa for providing his code and Prof. Kouno for making comments.

Appendix A: Jensen-Shannon divergence for A_y for 71 MeV

The Jensen-Shannon (JS) divergence consider two probabilities and make the comparison between their shapes quantitatively. We apply the JS divergence to A_y measured for $\vec{p}+{}^4\text{He}$ scattering at $E_{\text{lab}} = 72$ MeV and that for $\vec{p}+{}^6\text{He}$ scattering at $E_{\text{lab}} = 71$ MeV. This is a first application in nuclear physics. For this quantification, we start with two probability distributions, $p(q_i)$ and $q(q_i)$, having $0 \leq p(q_i) \leq 1$ and $0 \leq q(q_i) \leq 1$. The JS divergence is defined as [21]

$$D_{\text{JS}}(p||q) = \sum_{i=1}^N D_{\text{JS}}(q_i) \quad (\text{A1})$$

with

$$D_{\text{JS}}(q_i) = \frac{1}{2} \left[p(q_i) \ln \left(\frac{p(q_i)}{M(q_i)} \right) + q(q_i) \ln \left(\frac{q(q_i)}{M(q_i)} \right) \right], \quad (\text{A2})$$

for $M(q_i) = (p(q_i) + q(q_i))/2$. The $D_{\text{JS}}(p||q)$ satisfies

$$D_{\text{JS}}(p||q) = D_{\text{JS}}(q||p), \quad 0 \leq D_{\text{JS}}(p||q) \leq \ln 2 = 0.693. \quad (\text{A3})$$

The D_{JS} is finite; note that the word ‘‘divergence’’ maintains for historical reasons. When the probability distributions are perfectly matched with each other, the D_{JS} becomes exactly zero. The D_{JS} becomes $\ln 2 = 0.693$, when there are no overlap between the probability distributions.

In the present data analysis, the number N of data is 5. The $\{p_i\}$ are a normalized distribution of measured $(A_y + 1)/2$ for ${}^4\text{He}$, while the $\{q_i\}$ are a normalized distribution of measured $(A_y + 1)/2$ for ${}^6\text{He}$. The reason why we take $(A_y + 1)/2$ is that $0 \leq (A_y + 1)/2 \leq 1$.

Our result $D_{\text{JS}} \approx 0.0028$ is much smaller than $\ln 2 = 0.693$. This indicates that the shapes of the two probabilities are closed to each other. The average of $\{p_i\}$ ($\{q_i\}$) describes the magnitude M_4 (M_6) for ${}^4\text{He}$ (${}^6\text{He}$). The results are $M_4 = 2.434$ and $M_6 = 2.539$. The two magnitudes are closed to each other, since the difference $(M_6 - M_4)/M_6$ is 4 %.

When the two magnitudes are close to each other, we can improve the JS divergence as

$$D_{\text{JS}}(p||q)M_{\text{av}} = \sum_{i=1}^N D_{\text{JS}}(q_i)M_{\text{av}} \quad (\text{A4})$$

with

$$\begin{aligned} & D_{\text{JS}}(q_i)M_{\text{av}} \\ & \approx \frac{1}{2} \left[A_y^1(q_i) \ln \left(\frac{2A_y^1(q_i)}{A_y^1(p_i) + A_y^1(q_i)} \right) \right. \\ & \quad \left. + A_y^1(p_i) \ln \left(\frac{2A_y^1(p_i)}{A_y^1(p_i) + A_y^1(q_i)} \right) \right], \quad (\text{A5}) \end{aligned}$$

for the average $M_{\text{av}} = (M_4 + M_6)/2$. and $A_y^1(q_i) \equiv (A_y(q_i) + 1)/2$. The $D_{\text{JS}}(p||q)M_a$ describes the magnitude and the shape fo two curves. Our result is $D_{\text{JS}}(p||q)M_a = 0.007$ that is much smaller than the maximum $\ln 2 * M_a = 1.7236$. The improved JS divergence thus yields the same conclusion as the original JS divergence. The measured A_y for ${}^4,6\text{He}$ are thus close to each other, although the condition $U_{pn_1} = U_{pn_2} = 0$ is not good. There is no theory that explains the similarity.

Now we neglect the data at $q = 1.71 \text{ fm}^{-1}$. The result is $D_{\text{JS}}(p||q)M_a = 0.002$. This value is much smaller than $D_{\text{JS}}(p||q)M_a = 0.007$. The value of the $D_{\text{JS}}(p||q)M_a$ is much changed by the data at $q = 1.71 \text{ fm}^{-1}$. We hope that new measurements will be made for $\vec{p}+{}^4,6\text{He}$ scattering at 71 MeV

[1] M. Toyokawa, K. Minomo and M. Yahiro, Phys. Rev. C **88**, no. 5, 054602 (2013).
 [2] S. Watanabe *et al.*, Phys. Rev. C **89**, no. 4, 044610 (2014).
 [3] M. Hatano *et al.*, Eur. Phys. J. A **25**, 255 (2005).
 [4] T. Uesaka *et al.*, Phys. Rev. C **82**, 021602 (2010), [arXiv:1007.3775 [nucl-ex]].
 [5] S. Sakaguchi *et al.*, Phys. Rev. C **84**, 024604 (2011), [arXiv:1106.3903 [nucl-ex]].
 [6] S. Chebotaryov *et al.*, PTEP **2018**, no. 5, 053D01 (2018).
 [7] G. A. Moss, *et al.*, Phys. Rev. C **21**, 1932 (1980).
 [8] M. Burrows, C. Elster, S. P. Weppner, K. D. Launey, P. Maris, A. Nogga and G. Popa, Phys. Rev. C **99**, no. 4, 044603 (2019),

[arXiv:1810.06442 [nucl-th]].
 [9] R. Crespo and A. M. Moro, Phys. Rev. C **76**, 054607 (2007).
 [10] M. Gennari, M. Vorabbi, A. Calci and P. Navratil, Phys. Rev. C **97**, no. 3, 034619 (2018).
 [11] R. C. Johnson, J. S. Al-Khalili and J. A. Tostevin, Phys. Rev. Lett. **79**, 2771 (1997).
 [12] N. Yamaguchi, S. Nagata, and T. Matsuda, Progress of Theoretical Physics **70**, 459 (1983).
 [13] S. Nagata, M. Kamimura, and N. Yamaguchi, Progress of Theoretical Physics **73**, 512 (1985).
 [14] N. Yamaguchi, S. Nagata, and J. Michiyama, Progress of Theoretical Physics **76**, 1289 (1986).

- [15] T. Hamada and I. Johnston, Nuclear Physics **34**, 382 (1962).
- [16] M. Yahiro, K. Minomo, K. Ogata and M. Kawai, Prog. Theor. Phys. **120**, 767 (2008). [arXiv:0807.3799 [nucl-th]].
- [17] A. A. Korshennikov *et al.*, Nucl. Phys. A **617**, 45 (1997).
- [18] S. Burzynski, J. Campbell, M. Hammans, R. Henneck, W. B. Lorenzon, M. A. Pickar and I. Sick, Phys. Rev. C **39**, 56 (1989).
- [19] E. Hiyama *et al.*, Physical Review C **53**, 2075 (1996).
- [20] E. Hiyama, Y. Kino, and M. Kamimura, Progress in Particle and Nuclear Physics **51**, 223 (2003).
- [21] J. Lin, IEEE Transactions on Information theory, **37**, 145 (1991).
- [22] B. P. Abbott *et al.* [LIGO Scientific and Virgo Collaborations], Phys. Rev. X **9**, no. 3, 031040 (2019), [arXiv:1811.12907 [astro-ph.HE]].